



Article

A Multi-Frequency Omnidirectional Antenna Based on a Ring-Shaped Structure

Honglei Guo^{1,2,3,4}, Yu Chen^{1,2,3,4}, Qiannan Wu^{2,3,4,5,*}, Jianyang Wang^{2,3,4}, Yu He⁶, Yonghong Cao^{2,3,4,7} and Mengwei Li^{1,2,3,4,*}

¹ School of Instrument and Electronics, North University of China, Taiyuan 030051, China

² The Academy for Advanced Interdisciplinary Research, North University of China, Taiyuan 030051, China

³ The Center for Microsystem Integration, North University of China, Taiyuan 030051, China

⁴ College of Instrumentation and Intelligent Future Technology, North University of China, Taiyuan 030051, China

⁵ School of Semiconductor and Physics, North University of China, Taiyuan 030051, China

⁶ The MOE Key Laboratory of Weak-Light Nonlinear Photonics, TEDA Applied Physics Institute and School of Physics, Nankai University, Tianjin 300457, China

⁷ School of Aeronautics and Astronautics, North University of China, Taiyuan 030051, China

* Correspondence: qiannanwoo@nuc.edu.cn (Q.W.); lmwprew@163.com (M.L.)

Abstract: A multi-frequency microstrip antenna loaded with a ring-like structure has been proposed. The radiating patch on the antenna surface consists of three split-ring resonator structures, and the ground plate consists of a bottom metal strip and three ring-shaped metals with regular cuts to form a defective ground structure. The proposed antenna works in six different frequency bands covering 1.10, 1.33, 1.63, 1.97, 2.08, and 2.69 GHz and works entirely when connected to 5G NR (FR1, 0.45–3 GHz), 4GLTE (1.6265–1.6605 GHz), Personal Communication System (1.85–1.99 GHz), Universal Mobile Telecommunications System (1.92–2.176 GHz), WiMAX (2.5–2.69 GHz), and other communications frequency bands. Moreover, such antennas also have stable omnidirectional radiation properties across different operating frequency bands. This antenna meets the needs of portable multi-frequency mobile devices and provides a theoretical approach for the development of multi-frequency antennas.

Keywords: multi-frequency; microstrip antenna; split-ring resonator; defective grounding; omnidirectional radiation



Citation: Guo, H.; Chen, Y.; Wu, Q.; Wang, J.; He, Y.; Cao, Y.; Li, M. A Multi-Frequency Omnidirectional Antenna Based on a Ring-Shaped Structure. *Micromachines* **2023**, *14*, 994. <https://doi.org/10.3390/mi14050994>

Academic Editors: Ahmed A. Ibrahim and Syed Muzahir Abbas

Received: 8 April 2023

Revised: 30 April 2023

Accepted: 30 April 2023

Published: 3 May 2023



Copyright: © 2023 by the authors. Licensee MDPI, Basel, Switzerland. This article is an open access article distributed under the terms and conditions of the Creative Commons Attribution (CC BY) license (<https://creativecommons.org/licenses/by/4.0/>).

1. Introduction

In recent years, with the rapid development of wireless communication technology, wireless communication equipment is widely used in satellite navigation [1–3], wireless interconnection [4–7], high-speed information transmission, and other communication fields [8–12]. The antenna is an important component used to send and receive information in a wireless communication system [13,14]. The use of single-frequency antennas has been unable to meet the needs of modern multi-frequency communication. Moreover, when multiple antennas work at the same time in a limited space, there will be coupling effects between each other, resulting in the failure of the communication system to work normally. Modern wireless communication systems require antennas to be multifunctional, easy to integrate, low-cost, and miniaturized [15–18]. Multi-frequency antennas can work in multiple communication frequency bands at the same time. Moreover, using a single antenna to achieve multi-frequency effects, in a sense, greatly reduces the area of the antenna, saves the design cost, and meets the needs of industrial communication equipment [19–21]. Therefore, how to realize the multi-frequency radiation characteristics of antennae under other good conditions has become a hot research topic at present.

In recent years, various approaches have been developed to design and produce multi-frequency antennas. The main methods include the multilayer method [22–24], slot

method [25,26], branch method [27,28], the reconfigurable method [29–31], the metamaterial loading method [32–36], and Dipole multifrequency antenna [37–40]. For example, in 2010, Chen et al. [22] proposed a dual-frequency microstrip antenna using low-temperature co-fired ceramic (LTCC) technology by adopting a multi-layer method, which can be used for GPS positioning. In 2015, Wu et al. [25] proposed a multi-frequency antenna with three operating frequency points by etching three slots of different lengths on a triangular radiation patch. In 2018, Chun [28] designed an antenna composed of multiple branches. Changing the length of the corresponding branch effectively modulates the resonance frequency and impedance matching of the antenna. This antenna is an excellent choice for LTE, WLAN, WiMAX, and other narrowband systems. In 2018, Vijayan et al. [31] proposed a new antenna that uses two PIN diodes to modify the working state of the diode without changing the physical size of the antenna, which can obtain the reconfiguration of the antenna in four different frequency bands. In 2017, Rani [33] designed a metamaterial structural unit as the radiation patch of the antenna to obtain dual-frequency performance. In 2019, Zhang et al. [34] achieved dual-frequency operation by loading a transmission line-inspired structure onto the antenna. In 2020, a four-port four-frequency antenna available at high-low frequencies was presented by Chen et al. [37]. In 2021, Wan, S.Y. et al. [38] designed a multi-frequency microstrip antenna that works at seven frequency bands. In 2022, Anupa Chatterjee et al. [39] demonstrated a four-band compact dual-element MIMO (multi-input multi-output) antenna system consisting of a compact inverted F antenna with a zigzag arm. One side of the T-type monopole antenna is extended and twisted, and the other side is grounded, forming the IFA structure. In 2023, Fatma Taher et al. [40] designed a dual-port MIMO antenna that provided broadband of 25.5–30 GHz and a peak gain of 8.75 dBi. However, the above-proposed antennas could not meet the requirements of industrial communication equipment for multi-frequency communication in terms of multi-band, size, and gain for most of the operating frequency bands of multi-frequency antennas mentioned above.

In this paper, we introduce a new multi-frequency antenna structure, which can realize the function of the multi-frequency antenna at six frequency points. This method can improve the design of multi-frequency communication equipment.

2. Theory and Design

The geometry of the antenna simulation model is shown in Figure 1. The antenna is printed on a 1.6 mm thick Taconic RF-60A substrate with a relative dielectric constant of 6.15 and a loss angle of 0.0028. The printed metal is copper with a thickness of 0.036 mm. Three open-loop resonator structures are loaded on the front in the form of radiation patches, as shown in Figure 1b, and circular defect ground structures with cross-shaped cross notches and rectangular ground structures are distributed in corresponding positions on the back, as shown in Figure 1c. The entire open ring resonator radiation patch structure is connected to the feeder end via a microstrip line with an impedance set to 50 Ω . The parameters of the proposed antenna are given in Table 1.

Table 1. Design size of the multi-frequency antenna.

Parameter	L	W	h	R_1	R_2	R_3	u	r	g	c	m	t
Value/mm	60	42	1.6	7.5	13.5	19.5	3.17	1.5	1.5	1.5	1	0.036

The radiation patch on the front of the antenna structure consists of three split-ring resonator structures. When an electromagnetic wave is incident on an open resonant ring, the initially stable magnetic field induced by the incident wave changes and the magnetic field induces an induced current in the metal ring. The induced current flows over the metal ring such that the metal ring has an equivalent inductance. Moreover, due to the accumulation of charges between the metal rings, the metal rings generate equivalent inductance, and LC resonances occur in the metal rings [41]. According to the equivalence

principle of the open resonant ring, its resonant frequency can be expressed in the following formula [42].

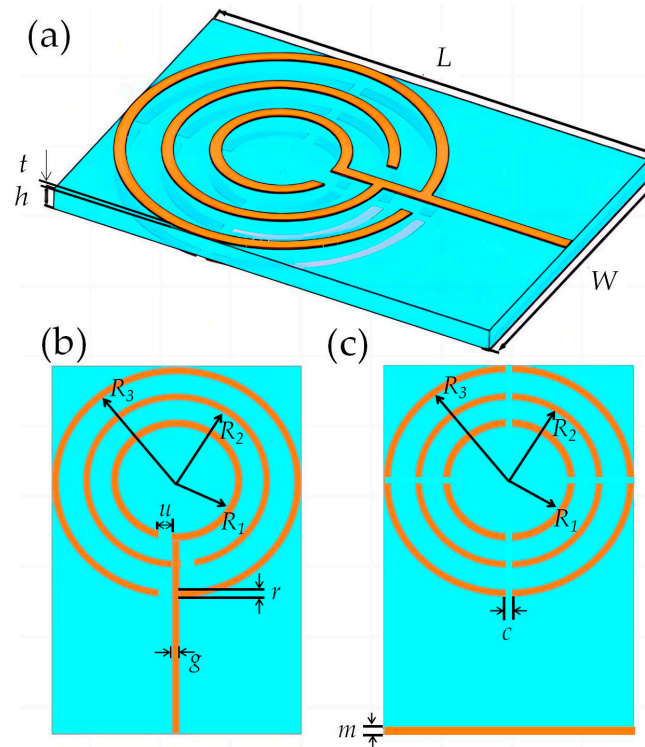


Figure 1. Antenna structure diagram. (a) Three-dimensional image of the antenna; (b) The front structure of the antenna; (c) The back structure of the antenna.

$$f_0 = \left[\sqrt{(C_{SRRs} R_{SRRs}^2) / L_{SRRs} - 1} \right] (2\pi C_{SRRs} R_{SRRs}) \tag{1}$$

Here, the L_{SRR} is the overall inductance of the SRRs, which is formed by the metal ring inductors in series with the current direction. C_{SRR} is the overall capacitance of the SRRs equivalent circuit. R_{SRR}^2 is the equivalent conductor loss, the shunt resistance. Its size is related to ring width g , metal thickness t , and metal material ρ .

The capacitance of the open resonant ring SRR_s is:

$$C_{SRRs} = (n - 1)[2R_1 - (2n - 1)(g + s)] / C_0 / 2 \tag{2}$$

$$R_{SRRs} = \rho[R_1 - (n - 1)(g + s)] / (gt) \tag{3}$$

$$L_{SRRs} = 4\mu_0[R_1 - (n - 1)(g + s)][\ln(0.98/\rho) + 1.84\rho] \tag{4}$$

where $n = 3$ is a ring number.

In the open resonant ring structure, the resonance effect is mainly generated by the outer ring. The inner ring is used to strengthen the coupling between the inner and outer rings so that the total capacitance of the open resonant ring structure is increased to achieve a shift of the resonant frequency to a lower frequency.

The inner split-ring resonator radius is R_1 , the middle split-ring resonator radius is R_2 , and the outer split-ring resonator radius is R_3 . The inner, middle, and outer radii of the proposed radiation patch are proposed from [35].

$$R_3 = \frac{29 \times 10^6}{f_0 \sqrt{\epsilon_{\text{reff}}}} \quad (5)$$

$$R_2 = 0.69R_3 \quad (6)$$

$$R_1 = 0.38R_3 \quad (7)$$

where f_0 is the lowest resonant frequency of the proposed antenna, and $\epsilon_{\text{reff}} = \sqrt{(\epsilon_r + 1)/2}$ is the effective dielectric constant of the substrate.

To explain the motives for developing the multi-frequency antenna, we show the process of antenna design more precisely. It should be emphasized that it is a common method to realize multi-frequency antennas by using multi-loop structures. Therefore, we compare the results of several multi-loop antennas here. Figure 2 shows the structural diagram of the evolution of a single-band antenna into a multi-band antenna. During the design process, we also discussed the influence of the shift of the antenna back structure on the antenna performance, among which, the simulation results of the back without a ring, three rings and three cross-shaped open rings have a similar trend, but the cross-shaped open ring structure makes the overall performance of the antenna optimal. Therefore, in this paper, we focus on the impact of the upper surface radiation patch structure on antenna performance. Figure 3 shows the simulation reflection coefficient (S_{11}) curve corresponding to the antenna evolution process.

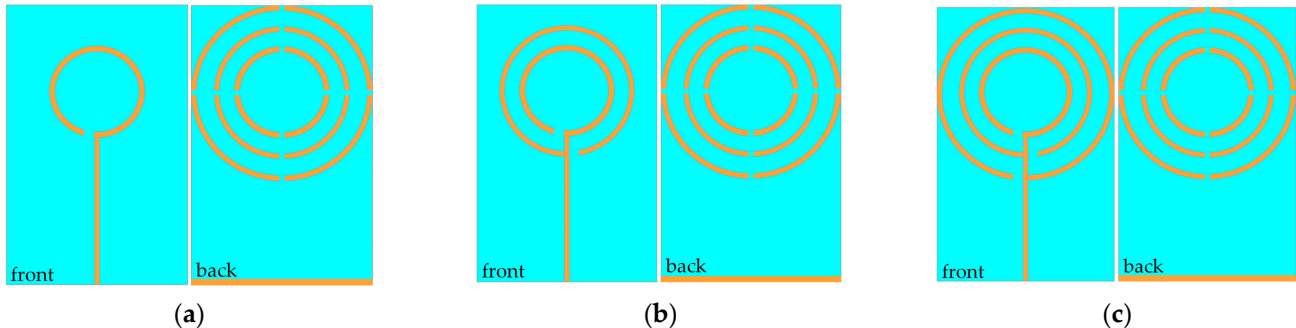


Figure 2. Antenna design process: (a) Single ring patch; (b) Double rings patch; (c) Three rings patch.

As shown in Figure 3a, the radiant patch is an open resonator with a single ring, and the resonant frequency of the antenna is only 0.38 GHz. Figure 3b shows the double-rings radiant patch. Since multi-frequency resonances can be achieved between circular split ring resonators of different sizes, the resonant frequencies of the antennas are 0.25, 0.53, 1.06, 1.46, and 2.03 GHz, but only at 2.03 GHz, the return loss (S_{11}) is less than -10 dB. Figure 3c based on the two becomes a three-ring open resonator radiation patch, enhancing the effect of multi-frequency resonance. Not only does the return loss (S_{11}) at the resonant points at 1.10, 1.32, and 2.07 GHz exceed 10 dB but new resonant points are added at 1.63, 1.97, and 2.9 GHz, indicating that the antenna has a multi-frequency capacity and can operate simultaneously in six bands from 0 to 3 GHz.

To better understand the reason for the multi-frequency radiation properties of the antenna, the surface current distribution of the antenna was simulated and analyzed at the following six frequencies: 1.10, 1.33, 1.63, 1.97, 2.08, and 2.69 GHz. The results are shown in Figure 4.

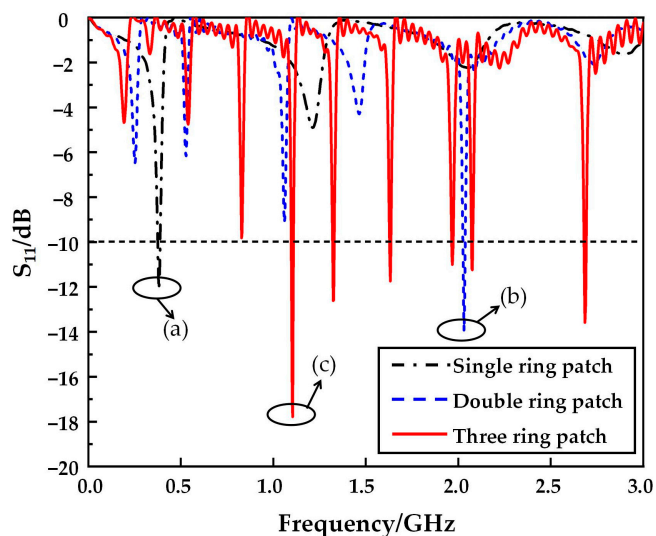


Figure 3. Simulation results of the return loss of three antennas. (a) Single ring patch; (b) Double rings patch; (c) Three rings patch.

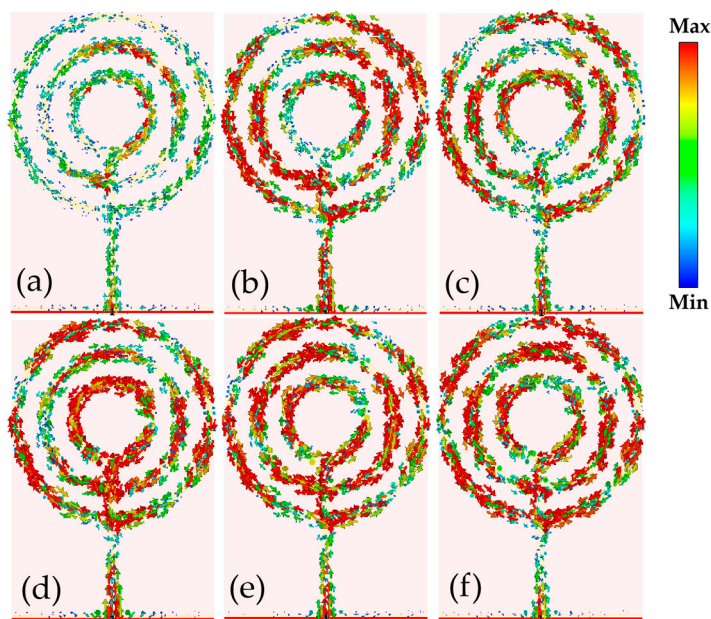


Figure 4. The surface current distribution of the antenna at (a) 1.10 GHz; (b) 1.33 GHz (c) 1.63 GHz; (d) 1.97 GHz; (e) 2.08 GHz; (f) 2.69 GHz.

As shown in Figure 4, the structure of the three open-loop resonators on the antenna surface. At lower frequencies, 1.10, 1.33, and 1.63 GHz. This suggests that, at lower frequencies, the outermost ring structure plays a major role in the emission. In the three higher frequency bands of 1.97, 2.08, and 2.69 GHz, the surface currents of the three open ring structures are uniform and high in density, so the three open ring structures act as radiation in the higher frequency bands.

Figure 5 shows the antenna radiation direction diagram in the E and H planes at six operating frequency points (1.10, 1.33, 1.63, 1.97, 2.08, and 2.69 GHz). As can be seen from Figure 5, when the antenna operates at 1.10, 1.33, and 1.63 GHz, surface E presents obvious “8” shaped half-wave dipole directional radiation characteristics, and the maximum radiation direction is near 0°. The orientation map of the surface H is approximately a positive circle, indicating that the antenna has omnidirectional radiation properties at this time. As the operating frequency changes from low to high, the direction of

antenna radiation changes to some extent. At 1.97 GHz, the antenna radiates approximately in the direction of the half-wave dipole radiation, and the radiation direction shift is negligible. However, in the two high-frequency operating bands of 2.08 and 2.69 GHz, the current distribution of the split-ring resonator ring structure on the antenna surface is more complex. The surface currents between the different ring structures affect each other, resulting in a shift of the maximum radiation direction of the antenna to the left. The higher the frequency, the larger the deviation angle, especially at 2.69 GHz where the back-lobe appears in the radiation direction map and directivity is slightly affected. However, in all three frequency bands, the maximum deviation of the radiation direction is small, and the H-plane orientation map is still approximately a positive circle, so the antenna still has omnidirectional radiation properties. Figure 6 shows the gain of the antenna in the operating frequency band, which reaches a maximum gain of 4.63 dBi. Overall, the proposed antenna has excellent omnidirectional radiation properties at all operating frequency points, which will meet the needs of portable multi-band mobile devices.

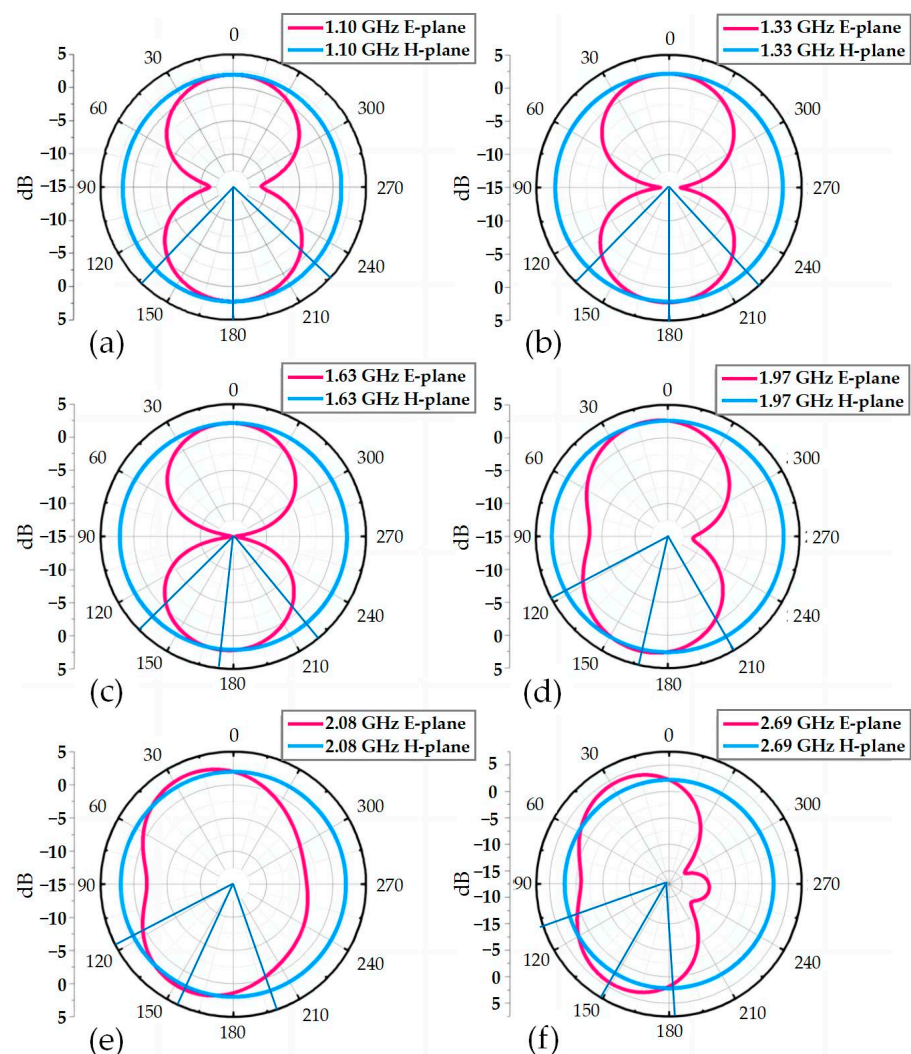


Figure 5. Antenna radiation direction diagram at (a) 1.10 GHz; (b) 1.33 GHz; (c) 1.63 GHz; (d) 1.97 GHz; (e) 2.08 GHz; (f) 2.69 GHz.

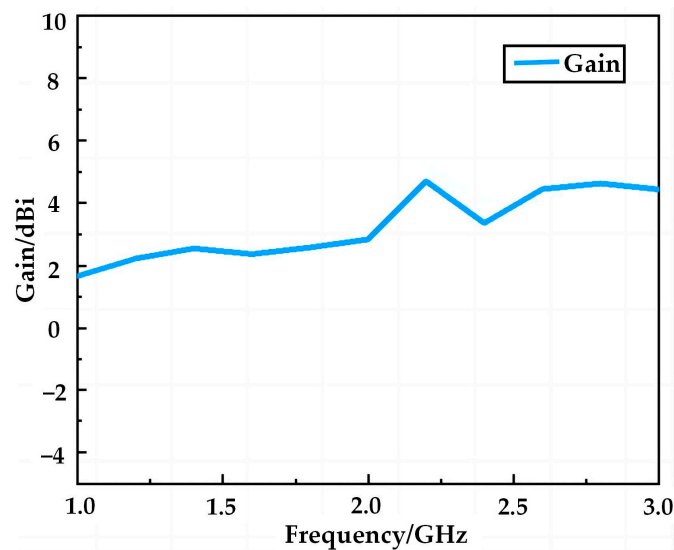


Figure 6. Simulation of antenna gain.

3. Test and Analysis

To verify the performance of the antenna, we use an electromagnetic computer simulation (CST) microwave studio to simulate and analyze the antenna parameters. The actual return loss (S_{11}) of the antenna is measured by an Agilent vector network analyzer under normal experimental conditions and compared with the simulation results. First, the microstrip line of the antenna is welded to the SMA joint matching the impedance of 50Ω . Then, the network analyzer is connected to a coaxial cable with the same impedance matching and calibrated in the order of open circuit-short circuit-load. After the device calibration, the antenna is connected with a coaxial cable and tested. The measurement of the antenna is shown in Figure 7.

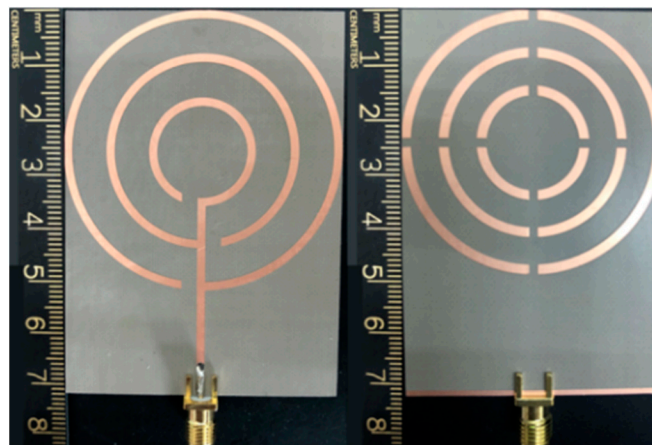


Figure 7. Photograph of the fabricated antenna.

The comparison between antenna simulation and measurement results is shown in Figure 8. The experimental results show that six frequency points can reach below 10 dB, and the number of frequency points is consistent with the six frequency points of the theoretical simulation. The six frequency points measured in the experiment are 0.58 GHz, 0.93 GHz, 1.23 GHz, 1.49 GHz, 2.42 GHz, 2.61 GHz, and the theoretical simulation is 1.10 GHz, 1.33 GHz, 1.63 GHz, 1.97 GHz, 2.08 GHz, 2.69 GHz respectively. There are three reasons why these frequencies are not the same. The first reason is the size error brought by processing. The second reason is the limitation of experimental conditions, the

measurements were not completed in the microwave darkroom, so the electromagnetic environment affected the antenna radiation. The third reason is that the SMA joint is not a perfect match with the sample.

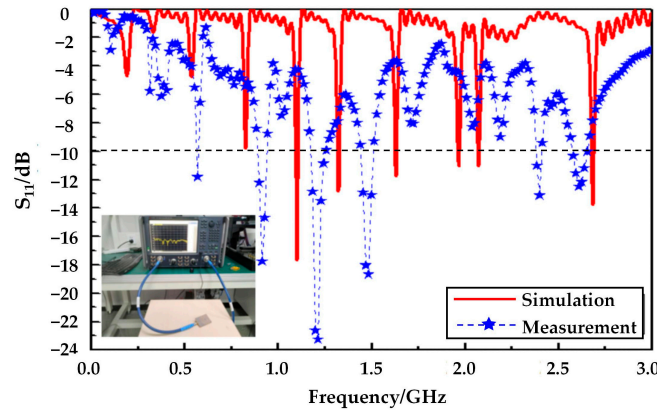


Figure 8. Simulated and measured reflection coefficient of the proposed antenna.

4. Comparison and Discussion

As can be seen from Table 2, the proposed antenna structure can achieve more operating frequency points while having higher gain compared to existing multi-frequency antennas, but the operating bandwidth at each resonant frequency point is slightly narrower, so there is still room for improvement.

Table 2. Research results of multi-frequency antennas.

Ref	Antenna Size Comparison (L × W mm ²)	Resonance Frequency f_0 (GHz)	The Number of −10 dB Bandwidth	−10 dB Bandwidth (GHz)	Maximum Gain
[6]	20 × 20	1.35/2.57/4.57/5.21	4	1.3–1.39/2.52–2.63/ 4.49–4.67/5.06–5.18	-
[15]	26 × 22	1.836/3.72/4.32	3	1.495–2.180/3.35–4.08/4.15–4.49	2.43 dBi
[20]	43.6 × 43.6	0.829/2.20/1.575/2.450	4	0.698–0.960/1.710–2.690/1.575/ 2.400–2.500	5.3 dBi
[22]	28.05 × 24.90	1.226/1.582	2	1.217–1.235/1.567–1.597	-
[24]	50 × 50	2.4/3.5/4.8	3	1.88–2.73/3.26–3.79/4.7–5.9	4.7 dBi
[25]	100 × 60	2.45/3.50/5.31	3	2.17–2.72/3.34–3.66/4.85–5.77	3.89 dBi
[27]	17 × 17	1.65/5.90	2	1.1–2.2/4.8–7.0	3 dBi
Proposed	62 × 42	1.10/1.33/1.63/ 1.97/2.08/2.69	6	1.097–1.109/1.319–1.329/ 1.628–1.635/1.964–1.971/ 2.071–2.078/2.679–2.691	4.63 dBi

5. Conclusions

In this paper, we design and simulate a new multi-frequency omnidirectional microstrip antenna using CST simulation software. The split-ring resonator structure on the antenna surface and the defect ground state structure on the back of the antenna can effectively control the surface current distribution and increase the resonant frequency of the antenna, effectively increasing the number of operating frequency bands. The measurements are in general agreement with the simulations. The proposed antenna can work nicely in 5G NR (FR1, 0.45–3 GHz), 4GLTE (1.6265–1.6605 GHz), Personal Communication System (1.85–1.99 GHz), Universal Mobile Telecommunications System (1.92–2.176 GHz), WiMAX (2.5–2.69 GHz), and other communication frequency bands. The antenna also has excellent omnidirectional radiation properties in different operating frequency bands, which meet the requirements of portable multi-band mobile devices and are of practical engineering interest and utility.

Author Contributions: Conceptualization, H.G., Y.C. (Yu Chen) and J.W.; methodology, H.G., Q.W. and Y.H.; software, Y.C. (Yu Chen) and J.W.; validation H.G. and Y.C. (Yu Chen); formal analysis, H.G. and Q.W.; investigation, J.W.; resources, Y.H.; data curation, H.G.; writing—original draft preparation, H.G.; writing—review and editing, Q.W., Y.C. (Yu Chen) and J.W.; visualization, Y.C. (Yonghong Cao); supervision, Y.C. (Yonghong Cao) and M.L.; project administration, M.L.; funding acquisition, Q.W. and M.L. All authors have read and agreed to the published version of the manuscript.

Funding: This research was funded by the Double First-Class Disciplines National First-Class Curriculum Construction, the National Future Technical College Construction Project, the Shanxi Province Postgraduate Education Reform Project, grant numbers 11013168 and 11013410, 11013169, 11012103 and 11012133.

Institutional Review Board Statement: Not applicable.

Informed Consent Statement: Not applicable.

Data Availability Statement: The data that support the findings of this study are available from the corresponding author upon reasonable request.

Conflicts of Interest: The authors declare no conflict of interest.

References

1. Liu, Y.T.; Shi, D.; Zhang, S.Y.; Gao, Y.G. Multiband antenna for satellite navigation system. *IEEE Antennas Wirel.* **2015**, *15*, 1329–1332. [[CrossRef](#)]
2. Zhang, H.L.; Hu, B.J.; Zhang, X.Y. Compact and broadband circularly polarized ring antenna with wide beam-width for multiple global navigation satellite systems. *Chin. Phys. B.* **2012**, *21*, 521–525. [[CrossRef](#)]
3. Falade, O.P.; Ur-Rehman, M.; Yang, X.D.; Safdar, G.A.; Parin, C.G.; Chen, X.D. Design of a compact multiband circularly polarized antenna for global navigation satellite systems and 5G/B5G applications. *Int. J. RF Microw. Comput.-Aided Eng.* **2020**, *30*, 22182. [[CrossRef](#)]
4. Yanikomeroglu, H.; Sousa, E.S. Antenna interconnection strategies for personal communication systems. *IEEE J. Sel. Areas Commun.* **2002**, *15*, 1327–1336. [[CrossRef](#)]
5. Bauernfeind, T.; Renhart, W.; Alotto, P.; Biro, O. UHF RFID antenna impedance characterization: Numerical simulation of Interconnection effects on the antenna impedance. *IEEE T Magn.* **2017**, *50*, 1204. [[CrossRef](#)]
6. Khan, I.; Ali, T.; Devanagavi, G.D.; Sudhindra, K.R.; Biradar, R.C. A compact multiband band slot antenna for wireless applications. *Internet Technol. Lett.* **2019**, *2*, 94. [[CrossRef](#)]
7. Sathikbasha, M.; Nagarajan, V. Design of multiband frequency reconfigurable antenna with defected ground structure for wireless applications. *Wirel. Pers. Commu.* **2020**, *113*, 867–892. [[CrossRef](#)]
8. Yan, K.Q.; Liu, H.D.; Ren, G.C.; Chen, J.; Chen, H.L. Information transmission policy for multi-antenna relay communication system with energy harvesting. *Commun. Technol.* **2016**, *49*, 576–581.
9. Xu, Q.; Zhou, H.C.; Hu, Y.W.; Fan, G.C.; Yan, Z.M.; Wang, Y. Windmill multifrequency antenna with split ring resonator. *Chin. J. Electron. Devices* **2019**, *42*, 557–562.
10. Muller, R. A random matrix model of communication via antenna arrays. *IEEE Trans. Inf. Theory.* **2002**, *48*, 2495–2506. [[CrossRef](#)]
11. Shui, M.Y.; Jiang, Z.N.; Li, X.Y.; Liang, Q.; Lu, X.C.; Liu, F. Analysis and design of a novel multi-frequency conformal microstrip antenna. *J. Hef. Univ. Technol.* **2018**, *41*, 800–804.
12. Zhou, L.; Tang, M.; Qian, J.W.; Zhang, Y.P.; Mao, J.F. Design of Heatsink Antennas for Integrated Systems. *Acta Electron. Sin.* **2022**, *50*, 1766–1773.
13. Row, J.S.; Ko, T.H. Broadband dual-polarized microstrip antenna fed with horizontal coaxial baluns. *Microw. Opt. Techn. Lett.* **2018**, *60*, 3053–3059. [[CrossRef](#)]
14. Singhal, S. Ultrawideband elliptical microstrip antenna for terahertz applications. *Microw. Opt. Technol. Lett.* **2019**, *61*, 2366–2373. [[CrossRef](#)]
15. Hussain, R.; Sharaw, M.S. An integrated slot-based frequency-agile and UWB multifunction MIMO antenna system. *IEEE Antennas Wirel. Propag. Lett.* **2019**, *18*, 2150–2154. [[CrossRef](#)]
16. Yasir, M.; Aldrigo, M.; Dragoman, M.; Dinescu, A.; Bozzi, M.; Iordanescu, S.; Vasilache, D. Integration of antenna array and self-switching graphene diode for detection at 28 GHz. *IEEE Electron Device Lett.* **2019**, *40*, 628–631. [[CrossRef](#)]
17. Kumar, A.; Naidu, P.V.; Kumar, V. A compact uniplanar ACS fed multi band low cost printed antenna for modern 2.4/3.5/5 GHz applications. *Microsyst Technol.* **2018**, *24*, 1413–1422. [[CrossRef](#)]
18. Liu, B.Y.; Jiang, Y.; Huang, Z.Y.; Chen, J.B.; Ye, Y.; Ji, P.F.; Xu, Q.H.; Wu, W.W.; Yang, J.J.; Yang, N.C. Miniaturization Design and Implementation of W-Band Micro-Coaxial Antenna Based on Wafer-Level Packaging. *Acta Electron. Sin.* **2022**, *50*, 1098–1106.
19. Cheng, J.H.; Song, H.H. Ultra-high frequency multiband antenna with stair shaped ground plane for radio frequency identification applications. *Microw Opt Technol. Lett.* **2017**, *59*, 2335–2340. [[CrossRef](#)]

20. Wei, D.L.; Nan, X.L.; Xia, P. The utility model relates to an L-type multi-band WLAN and WiMAX micro antenna. *Electron. Des. Eng.* **2023**, *31*, 7–10, 15.
21. Feng, Z.H.; Du, Z.W. Study on Novel Antennas and Channel Properties of SI SO/MI MO Systems. *Acta Electron. Sin.* **2007**, *35*, 7–12.
22. Chen, S.C.; Liu, G.C.; Chen, X.Y.; Lin, T.F.; Liu, X.G.; Duan, Z.Q. Compact dual-band GPS microstrip antenna using multilayer LTCC substrate. *IEEE Antennas Wirel. Propag. Lett.* **2010**, *9*, 421–423. [[CrossRef](#)]
23. Xu, Y.H.; Zhou, M.L.; Wang, A.Y.; Hou, J.Q. Design of a compact magneto-electric dipole antenna. *Microw Opt. Technol. Lett.* **2023**, 1–6. [[CrossRef](#)]
24. Zhang, Z.W.; Xu, Y.H.; Zhou, M.L.; Wang, A.Y. Design of mine multi-band microstrip antenna. *J. Mine Automation* **2022**, *48*, 125–129.
25. Wu, M.T.; Chuang, M.L. Multibroadband slotted bow-tie monopole antenna. *IEEE Antennas Wirel. Propag. Lett.* **2015**, *14*, 887–890. [[CrossRef](#)]
26. Avila, D.R.; Marrero, Y.P.; Vera, A.S.; Rizo, F.M.; Sanz, J.V.; Puente, A.T. Printed quad-band CPW-fed slot antenna. *Microw Opt. Technol. Lett.* **2016**, *58*, 145–151. [[CrossRef](#)]
27. Sedghi, T. Compact fractal antenna for WiMAX 1.4 GHz and IEEE 802.11a using double branch line. *J. Instrum.* **2018**, *13*, 09021. [[CrossRef](#)]
28. Chung, M.A. A miniaturized triple band monopole antenna with a coupled branch strip for bandwidth enhancement for IoT applications. *Microw Opt. Technol. Lett.* **2018**, *60*, 2336–2342. [[CrossRef](#)]
29. Zhang, X.Y.; Tian, M.; Zhan, A.; Liu, Z.W.; Liu, H.W. A frequency reconfigurable antenna for multiband mobile handset applications. *Int. J. RF Microw. Comput.-Aided Eng.* **2017**, *27*, 21143. [[CrossRef](#)]
30. Idris, I.H.; Hamid, M.R.; Kamardin, K.; Rahim, M.K.A. A multi to wideband frequency reconfigurable antenna. *Int. J. RF Microw. Comput.-Aided Eng.* **2017**, *28*, 21216. [[CrossRef](#)]
31. Arun, V.; Karlmarx, L.R.; Jegadish, K.J.K.; Christy, C.V. N-Shaped frequency reconfigurable antenna with auto switching unit. *Appl. Comput. Electrom.* **2018**, *33*, 710–713.
32. Raval, F.; Kosta, Y.P.; Joshi, H. Triple-band circular patch antenna using rising sun shaped metamaterial structure. *Int. J. Appl. Electrom.* **2014**, *46*, 501–509. [[CrossRef](#)]
33. Rani, R.B.; Pandey, S.K. ELC metamaterial based CPW-fed printed dual-band antenna. *Microw Opt. Technol. Lett.* **2017**, *59*, 304–307. [[CrossRef](#)]
34. Zhang, J.H.; Yan, S.; Vandenbosch, G.A.E. A Metamaterial inspired dual band frequency reconfigurable antenna with pattern diversity. *Electron. Lett.* **2019**, *55*, 573–574. [[CrossRef](#)]
35. Abbosh, A.M.; Bialkowski, M.E.; Mazierska, J.; Jacob, M.V. A planar UWB antenna with signal rejection capability in the 4–6 GHz band. *IEEE Microw. Wirel. Co.* **2006**, *16*, 278–280. [[CrossRef](#)]
36. Wu, X.L.; Zheng, Y.; Luo, Y.; Zhang, J.G.; Yi, Z.; Wu, X.W.; Cheng, S.B.; Yang, X.W.; Yu, Y.; Wu, P.H. A four-band and polarization-independent BDS-based tunable absorber with high refractive index sensitivity. *Phys. Chem. Chem. Phys.* **2021**, *23*, 26864–26873. [[CrossRef](#)]
37. Chen, C.H.; Lin, Y.F.; Huang, P.W.; Chen, H.M.; Liao, C.T. Design of multi-band antenna for LTE wearable device with shared slots and radiators for smart watch. *Int. J. RF Microw. Comput.-Aided Eng.* **2020**, *30*, 22415. [[CrossRef](#)]
38. Wan, S.Y.; Wang, D.Q.; Luo, S. Design of Multi-frequency Microstrip Antenna based on Metamaterial. *Study Opt. Commun.* **2021**, *4*, 72–78.
39. Chatterjee, A.; Midya, M.; Mishra, L.P.; Mitra, M. Two-Element Quad-Band MIMO Antenna Employing Meandered Arm Printed Inverted-F Antenna. *Wirel. Pers. Commun.* **2022**, *126*, 511–529. [[CrossRef](#)]
40. Taher, F.; Hamadi, H.A.; Alzaidi, M.S.; Alhumyani, H.; Elkamchouchi, D.H.; Elkamshoushy, Y.H.; Haweel, M.T.; Sree, M.F.A.; Fatah, S.Y.A. Design and Analysis of Circular Polarized Two-Port MIMO Antennas with Various Antenna Element Orientations. *Micromachines* **2023**, *14*, 380. [[CrossRef](#)]
41. Shamonin, M.; Shamonina, E.; Kalinin, V.; Solymar, L. Resonant frequencies of a split-ring resonator: Analytical solutions and numerical simulations. *Microw Opt. Technol. Lett.* **2005**, *44*, 133–136. [[CrossRef](#)]
42. Bie, S.H.; Pu, S.; Xiong, J.Y. A novel terahertz dual-frequency microstrip antenna array. In Proceedings of the 2021 Altair Technology Conference 2021, Paris, France, 16–18 October 2021; pp. 140–150.

Disclaimer/Publisher’s Note: The statements, opinions and data contained in all publications are solely those of the individual author(s) and contributor(s) and not of MDPI and/or the editor(s). MDPI and/or the editor(s) disclaim responsibility for any injury to people or property resulting from any ideas, methods, instructions or products referred to in the content.